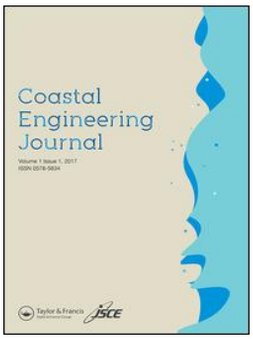

Coastal Engineering Journal

ISSN: (Print) (Online) Journal homepage: https://www.tandfonline.com/loi/tcej20

Development of a fully coupled wind stress-wave-ocean coastal model system

Peng Zheng, Ming Li, Jianting Du, Caixia Wang, Judith Wolf & Xueen Chen

To cite this article: Peng Zheng, Ming Li, Jianting Du, Caixia Wang, Judith Wolf & Xueen Chen (2023): Development of a fully coupled wind stress-wave-ocean coastal model system, Coastal Engineering Journal, DOI: 10.1080/21664250.2023.2179791

To link to this article: https://doi.org/10.1080/21664250.2023.2179791

Published online: 25 Feb 2023.

COASTAL ENGINEERING JOURNAL
https://doi.org/10.1080/21664250.2023.2179791

Development of a fully coupled wind stress-wave-ocean coastal model system

Peng Zheng[a], Ming Li[b], Jianting Du[c], Caixia Wang[d], Judith Wolf[e] and Xueen Chen[f]

[a]Key Laboratory of Environmental Protection Technology on Water Transport, Ministry of Transport, Tianjin research institute for water transport engineering, M.O.T, Tianjin, China; [b]School of Engineering, University of Liverpool, Liverpool, UK; [c]First Institute of Oceanography, Ministry of Natural Resources, Qingdao, China; [d]Tianjin Binhai New Area Bureau of Meteorology, Tianjin, China; [e]National Oceanography Centre, Liverpool, England, UK; [f]Multispheres and Earth System (FDOMES) and Physical Oceanography Laboratory, Ocean University of China, Qingdao, China

ABSTRACT

To conserve momentum flux across the air-sea interface, a new wind stress-wave-ocean coupled coastal model system is developed. Via simulating a specific idealized tropical cyclone (TC), this model is firstly applied to study the impacts of three wave effects, including the commonly studied wave-breaking induced acceleration, wave-enhanced bottom friction and the seldom studied wave modified surface stress (WMWS), and the conservation of momentum flux across air-sea interface (MFB) on the predictions of storm surge and inundation. It is then further applied to investigate the role of above four effects in modeling the peak surge and inundation by generalizing the TC forcing with various physical parameters, including the TC intensity, size, translation speed, and bottom slope. The model results reveal that WMWS can contribute considerably to the total surge height and inundation distance in a relatively high-intensity TC and its contribution depends weakly on the varying bottom slopes, TC sizes or translation speeds. By contrast, the MFB can only considerably reduce the maximum storm surge with a small bottom slope, while its reduction on inundation distance is more significant. The present study thus highlights the importance and necessity of incorporating the commonly ignored effects of WMWS and MFB in coastal modeling.

ARTICLE HISTORY
Received 20 October 2022
Accepted 7 February 2023
Published online

KEYWORDS
Wind stress-wave-ocean coupled model; WBLM model; air-sea momentum flux budget; storm surge

1. Introduction

The wind waves is one of the most pronounced phenomena in the interface between lower atmosphere and upper ocean, the effects of which produce the connections in the large-scale oceanic and atmospheric systems (Babanin, Onorato, and Qiao 2012). On the one hand, wind waves constantly interact with subsurface ocean currents and drive many unique flow features in shallow coastal seas (e.g. alongshore current, rip current and undertow) and various upper-ocean mixing related issues (e.g. deepening of the upper mixed layer) in the deep ocean. Surface waves also distort the wind profiles near the ocean surface and affect the magnitude and distribution patterns of the wind stress. The interactions between wind stress, surface waves, and subsurface currents are considered to be significant to both ocean and atmospheric dynamics.

One prominent example of such wind stress-wave-ocean circulation interactions is the typhoon or severe storm-induced strong currents and devastating surge in the coastal region. Most existing research, however, relies on an ocean circulation model or a wave-current coupled model to study the surge (Dietrich et al. 2012; Wang and Sheng 2016; Zheng et al. 2020; Mao and Xia 2017; Zheng et al. submitted), with simple descriptions of the wind stress as a monotonic growth function of the neutral 10/m wind speed (e.g. Large and Pond 1981; Wu 1982), while only few studies took into account the effect of sea state (surface waves fields) on the wind stress. It has long been recognized (e.g. Monin and Mikhalovich Obukhov 1954; Charnock 1955) that the surface wave fields (and also ocean currents) can significantly modify the wind stress (or the drag coefficient C_d, or the surface roughness length z_0), which in turn dominates the wave growth and drives the ocean currents. Therefore, the dynamics of wind stress, waves and currents are closely linked with each other, and an accurate evaluation of the wind stress is of great importance for not only the wave-current coupled dynamics but also other related processes (e.g. storm surges, inundation) in the coastal environments.

To better evaluate the wind stress, numerous studies in the literature (e.g. Donelan et al. 1993; Taylor and Yelland 2001; Drennan, Taylor, and Yelland 2005) have been conducted to parameterize C_d through extra wave parameters (e.g. the inverse wave age u_*/c_p, the wave steepness H_s/L_p) in addition to the 10 m wind speed. However, such parameterizations often are fitted to limited measurements and thus are unable to represent the complex and fast changing wind and wave conditions, especially for those in coastal areas during storms (Du, Bolaños, and Guo

CONTACT Peng Zheng zp112academic@gmail.com; XueenChen xchen@ouc.edu.cn

Larsén 2017; Chen, Hara, and Ginis 2020). Furthermore, the dependence of C_d on wind speed and finite wave parameters is found to be scattered significantly against the measured data, suggesting additional processes and physical properties also contribute considerably to the wind stress (Babanin and Makin 2008). To reduce these uncertainties, one feasible approach is to explicitly model wind stress based on the full wave spectrum by directly coupling a wave model with the surface wave boundary layer model (WBLM; Babanin, Onorato, and Qiao 2012; Reichl, Hara, and Ginis 2014; Chen, Hara, and Ginis 2020). By taking into account of conservation of both the momentum and kinetic energy in the surface wave boundary layer (WBL; the lower part of the atmospheric boundary layer over the ocean surface, which is significantly affected by the surface waves) in addition to the spectral sheltering effect, the WBLM (Hara and Belcher 2004; Moon, Ginis, and Hara 2004) has the advantage of explicitly solving the physical details of various air-sea interaction processes, whereby the wind stress can be directly obtained as shown in plentiful of previous studies, e. g. Moon, Ginis, and Hara (2004); Moon et al. (2009); Chen and Xiping (2016), Chen and Xiping (2017); Du, Bolaños, and Guo Larsén (2017); Jianting et al. (2019); Chen, Ginis, and Hara (2020); Chen, Hara, and Ginis (2020). Specially, by using this WBLM model to investigate the shoaling-waves modified wind stress in coastal waters during uniform wind and tropical cyclones (TC), Chen, Ginis, and Hara (2020); Chen, Hara, and Ginis (2020) showed that the sea-state dependence of wind stress magnitude (or C_d) is significantly increased in shallow waters.

Storm surges are abnormal variations of sea level driven by atmospheric forcing associated with extratropical storms or TC (Zheng et al. 2020), including wind-, pressure- and wave-driven components (setup) but not the effects of tides or wave run-up (Wu et al. 2018). The surface waves can affect the storm surge through three aspects, i.e. the wave modified surface stress, wave-breaking induced acceleration (hereinafter WBA, or wave radiation stress) and wave-enhanced bottom friction (hereinafter WEB), and it has been widely acknowledged to be an important factor affecting the storm surges. However, most previous studies only highlighted the contributions of WBA (or the combination of WBA and WEB) to storm surge. There are few studies investigating the effect of wave modified surface wind stress, which is expected to be significant in shallow waters due to the large impact of shoaling surface waves on the wind stress (Chen, Ginis, and Hara 2020; Chen, Hara, and Ginis 2020). It is thus questionable to neglect the effect of wave modified wind stress (hereinafter WMWS) in storm surge models. Furthermore, less attention is paid to the overall three wave effects on the storm surge and the associated overland inundation. TC-induced storm surge and resulting inundation can bring devastating damage to coastal areas. Fully incorporating the wave effects in storm surge and inundation modelings is thus of great importance for real-time forecast and associated hazard early warning, as it can improve the description of underlying physics and hence the accuracy of model results.

In an ocean model, the momentum flux into the subsurface ocean currents (seaside stress) is commonly taken to be identical to the total (air-side) wind stress, with the assumption that no net momentum flux is acquired or lost by the surface waves. Such an assumption is only valid over a fully developed wave field, when the wave absorbed momentum from the wind field and wave dissipated momentum to the ocean are in equilibrium. In most of the situations, however, this is not satisfied (Janssen 2012), especially under TC conditions when the wave field is complicated and spatially and temporally fast varying. Depending on whether the wave field is growing or decaying, the seaside stress can be significantly less or higher than the air-side wind stress. Therefore, an air-sea momentum flux budget analysis is clearly needed, following which the conservation of momentum flux across the air-sea interface can be guaranteed, especially in a coupled model system. However, to what extent the model results can be improved is not clear.

The present study therefore aims to develop a fully coupled wind stress-wave-ocean coupled model, which is applicable to calculate the wave modified wind stress in both the shallow and deep waters via taking account of the complicated wind stress-wave-ocean interactions, and at the same time conserving the total momentum flux across the air-sea interface between atmosphere and ocean. This developed model system is subsequently used to investigate and quantify the impacts of different wave effects on storm surge and overland inundation with systematic idealized numerical experiments. The remaining of this paper is organized as follows. Section 2 describes in detail the wind stress-wave-ocean coupled model developed in this study. The specially designed experiment used to examine the impact of three wave effects and the momentum flux conservation across air-sea interface on the storm surge and coastal inundation modeling with different TC characteristics and topography features are described in Section 3. The relevant results are detailed and analyzed in Section 4, with major findings concluded in Section 5.

2. The wind stress-wave-ocean coupled model

Zheng et al. (2017) developed a three-dimensional wave-ocean fully coupled model system by coupling the unstructured grid version of the third-generation spectral wave model (UnSWAN; Zijlema 2010) into the three-dimensional ocean circulation model FVCOM

(Chen, Liu, and Beardsley 2003). This model adopted the vortex-force scheme to represent the wave-current interactions, modified the Generic Length Scale (GLS) turbulence scheme to better reproduce the wave-breaking enhanced turbulence together with a roller transport model to account for the effect of surface wave rollers, and also took into account the wave enhanced bottom stress. It has been validated by ideal and laboratory experiments and successfully applied to study the detailed hydrodynamics of the Pearl River Estuary during the TC Hato (Zheng et al. 2020; De Dominicis et al. 2020; Zheng et al. submitted). However, it is noted that this model utilized a bulk formula (Large and Pond 1981) to evaluate the wind stress, which does not account for the significant interactions between the wind stress and wave fields and also not appropriate to be used in high wind (e.g. TC) conditions. Therefore, in this study, we further extend it into a wind stress-wave-ocean coupled model system by conducting the followings:

(1) Adapting and coupling the WBLM (Chen, Ginis, and Hara 2020; Chen, Hara, and Ginis 2020) into the model system, in the meantime implementing a bulk C_d formulation that is applied in the current NOAA HWRF hurricane prediction model (hereinafter bulk-HWRF formulation, Biswas et al. (2018)) for comparative study purpose; and
(2) Including a flux budget module to guarantee the conservation of momentum flux across the air-sea interface.

The structure and main modules included in the new wind stress-wave-ocean coupled model system are shown in Figure 1. In the following section, the WBLM and sea surface momentum flux budget modules are described in detail. The other modules, which have been presented in (Zheng et al. 2017), are only briefly discussed for the sake of completeness herein.

2.1. Wave model

The wave action balance equation in UnSWAN is represented as

$$\frac{\partial N}{\partial t} + \quad _{\perp} \cdot \left[(C_g + V)N\right] + \frac{\partial c_\theta N}{\partial \theta} + \frac{\partial c_\sigma N}{\partial \sigma} = \frac{S_{tot}}{\sigma} \qquad (1)$$

where $N(\sigma, \theta; x, y, t) = E/\sigma$ is the action density spectrum, $E(\sigma, \theta; x, y, t)$ is the energy density spectrum; c_θ and c_σ are the propagation velocities in spectral space (θ, σ); θ is wave propagation direction and σ is wave radian frequency; $C_g = \partial\sigma/\partial k$ is the group velocity, k is the wave number vector, V is the ambient water current vector, $_{\perp}$ is the horizontal differential operator, $S_{tot}(\sigma, \theta)$ is the source-sink term which could be represented as

$$S_{tot} = S_{in} + S_{nl3} + S_{nl4} + S_{ds,w} + S_{ds,b} + S_{ds,br} \qquad (2)$$

where the first term denotes the wind energy input, the second and third terms represent the wave energy distribution through three-wave (triad) and four-wave (quadruplet) interactions, and the last three terms represent the wave energy dissipation caused by white-capping, bottom friction, and depth-induced wave breaking.

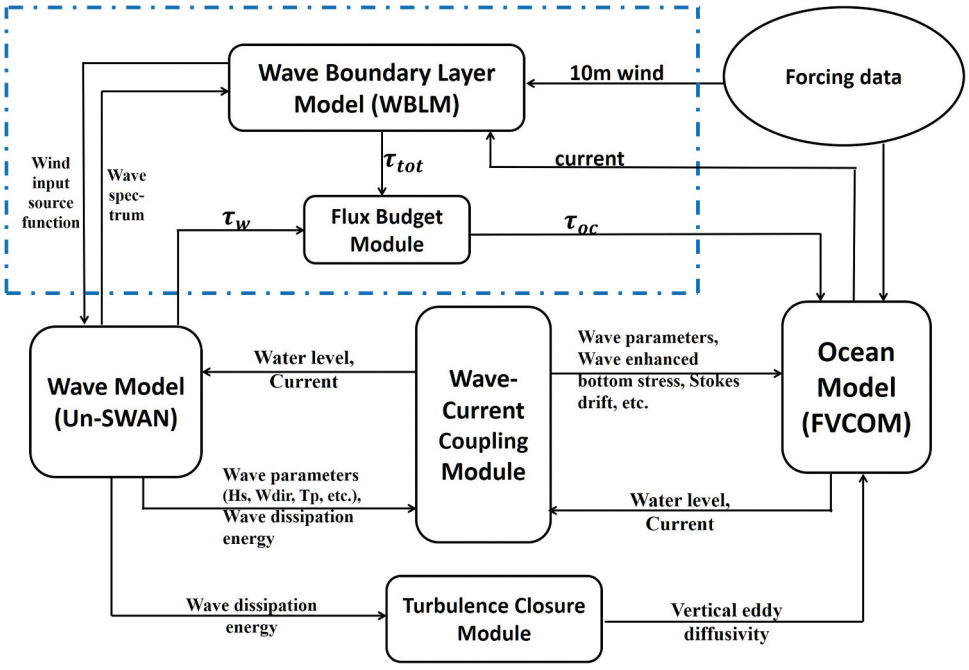

Figure 1. A schematic diagram on the structure of the wind stress-wave-ocean coupling model system; the modules inside the blue dashed box represent the newly developed components in this study, while the other components outside the blue box represent the previously developed wave-ocean coupled model by Zheng et al. (2017).

In this study, all of the above six terms are activated and are calculated with their default parameterization methods and relevant parameters as in the official UnSWAN model of version 41.20A (The SWAN Team 2018). The wave simulations are conducted with 72 equally spaced directional bins and 40 frequency bins starting at 0.0285 with a logarithmic increment factor of 1.1. It should be noted that the UnSWAN model does not explicitly resolve the high-frequency range of the wave spectrum (the spectral tail), which is, however, reported to be highly important for the wind stress calculations (Reichl, Hara, and Ginis 2014; Chen, Hara, and Ginis 2020). Therefore, the unresolved high-frequency spectral tail in the present model system is parameterized as a function of wind speed following Chen, Hara, and Ginis (2020) (c.f. their Section 3.2.1), by tuning the value of directionally integrated saturation spectrum (B_{sat}) so that the calculated sea-state-dependent C_d is consistent with a given bulk C_d formulation (bulk-HWRF formulation in this study) on average. After the high-frequency spectral tail is obtained, it is attached to the resolved part of UnSWAN spectrum to construct the complete wave spectrum following the same method as shown in Reichl, Hara, and Ginis (2014), which will later be used to calculate the sea-state-dependent wind stress by the WBLM method.

2.2. Ocean model

Following Zheng et al. (2017), the 3D momentum and continuity equations for wave-averaged currents, including the Vortex Force formalism (McWilliams, Restrepo, and Lane 2004; Uchiyama, McWilliams, and Shchepetkin 2010) and the WEC terms (at right-hand side of equation), are given by:

$$\begin{cases} \frac{\partial V}{\partial t}+(V\cdot\ _{\perp})V+w\frac{\partial V}{\partial z}+f\hat{z}\times V+\ _{\perp}\phi-F-\frac{\partial}{\partial z}\left(K_m\frac{\partial V}{\partial z}+v\frac{\partial V}{\partial z}\right) \\ =-\ _{\perp}\mathcal{K}-\hat{z}\times V^{st}\left(f+\left(\hat{z}\cdot\ _{\perp}\times V\right)\right)-w^{st}\frac{\partial V}{\partial z}+F^{w} \\ \frac{\partial \phi}{\partial z}+\frac{g\rho_w}{\rho_{w0}}=-\frac{\partial \mathcal{K}}{\partial z}+V^{st}\cdot\frac{\partial V}{\partial z} \\ \ _{\perp}\cdot V+\frac{\partial w}{\partial z}=0 \end{cases} \tag{3}$$

In the above equations the boldface typeset is used for the horizontal vectors, while the vertical components are represented by a normal typeset so that the 3D vectors are designated by (**horizontal**, vertical). (V, w) and (V^{st}, w^{st}) are the Eulerian mean and Stokes velocities, respectively; f is the Coriolis parameter; ϕ is the dynamic pressure (normalized by the density ρ_0); F represents the non-wave non-conservative forces and F^w represents the wave-induced non-conservative forces; ρ_w and ρ_{w0} are total and reference densities of sea water respectively; g is the gravity acceleration. The vertical coordinate range is $-h(\mathbf{x}) \le z \le \zeta+\hat{\zeta}$, in which ζ and $\hat{\zeta}$ are the mean and quasi-static sea-level components, respectively. $\mathcal{K}$ is the lower order Bernoulli head (after removing quasi-static terms, McWilliams, Restrepo, and Lane 2004) and is expressed as:

$$\mathcal{K}=\frac{1}{32}\frac{\sigma H_s^2}{k\sinh^2[kD]}\int_{-h}^{z}\frac{\partial^2 \Upsilon}{\partial z'^2}\sinh[2k(z-z')]\,dz' \tag{4}$$

where $\Upsilon = k\cdot V$.

The non-conservative wave acceleration term F^w originates from the transferring of momentum from surface waves to the subsurface ocean, including the momentum acceleration that induced by the white-capping, depth-induced wave breaking, and bottom friction. It is expressed as

$$F^{w}=g\int_0^{\infty}\int_{-\pi}^{\pi}\frac{k}{\sigma}\left[\left(S_{ds,w}+S_{ds,br}\right)f^{sf}(z)+S_{ds,b}f^{bf}(z)\right]d\theta d\sigma \tag{5}$$

where $f^{sf}(z)$ and $f^{bf}(z)$ are the empirical vertical distribution functions that quantify the vertical penetration of momentum associated with surface breaking waves and the upward decaying of momentum associated with bottom friction, respectively. The $f^{sf}(z)$ is given by

$$f^{sf}(z)=\frac{\cosh[k_{sf}(h+z)]}{\int_{-h}^{\zeta^c}\cosh[k_{sf}(h+z)]dz} \tag{6}$$

where $k_{sf}^{-1}=a_{sf}H_{rms}$ is a decay parameter that controls the penetration depth; H_{rms} is root mean square wave height; a_{sf} is an empirical constant and is set to 0.2 in this study; $\zeta^c=\zeta+\hat{\zeta}$ is the composite sea level. $f^{bf}(z)$ is given by

$$f^{bf}(z)=\frac{\cosh[k_{bf}(z^c-z)\ ]}{\int_{-h}^{\zeta^c}\cosh[k_{bf}(\zeta^c-z)\ ]dz} \tag{7}$$

with a decay length $k_{bf}^{-1}=a_{bf}\delta_w$, where a_{bf} is an empirical constant which is equal to one under monochromatic waves and has a much larger value (e.g. $a_{bf}=3$ is used in this study following Reniers et al. (2004)) under random waves; δ_w is the wave bottom boundary layer thickness and is expressed as a function of the semi-orbital excursion length (A_b), Nikuradse roughness (k_N) and bottom roughness length (z_{0b}).

The body force F^w can also be represented as an equivalent boundary stress:

$$\begin{aligned}\tau^{swd}&=\rho_{w0}D\overline{F^w}\\&=\rho_{w0}g\int_0^{\infty}\int_{-\pi}^{\pi}\frac{k}{\sigma}\left(S_{ds,w}+S_{ds,br}+S_{ds,b}\right)d\theta d\sigma\end{aligned} \tag{8}$$

where $\overline{F^w}$ represents the depth-averaged F^w; $D=h+\zeta^c$ is the wave-averaged thickness of the water column.

For a more detailed description of this ocean model, including the modified GLS turbulence model, roller

transport model and wave enhanced bottom stress, the reader is referred to Zheng et al. (2017).

2.3. Wave boundary layer model

The WBLM used in this study is based on Reichl, Hara, and Ginis (2014) for investigation of sea-state-dependent wind stress in deep waters under steady uniform winds and hurricane winds, which is further extended to the finite and shallow waters by Chen, Ginis, and Hara (2020); Chen, Hara, and Ginis (2020) to study the impact of shoaling surface waves on wind stress. In this approach, the combination of momentum conservation and energy conservation inside the WBL is adopted, e.g. the conservation of momentum requires the total momentum flux (total air-side wind stress) τ_{tot}, which is the sum of the wave-induced stress $\tau_w(z)$ and the turbulent stress $\tau_t(z)$, is constant with height within the WBL:

$$\tau_{tot} = \tau_w(z) + \tau_t(z) = \text{constant} \tag{9}$$

Similarly, the conservation of energy means that

$$\frac{d(\mathbf{U}\cdot\tau_{tot})}{dz} + \frac{d\Pi_w}{dz} - \rho_a\varepsilon = 0 \tag{10}$$

where $\mathbf{U}$ is the mean wind velocity; Π_w is the vertical transport of the kinetic energy related to the wave-induced motions; ρ_a is the air density; ε is the viscous dissipation of TKE.

The wave-induced stress τ_w (z) at height z is equal to the integration of momentum flux to the waves with the range of $\sigma_{min} \le \sigma \le \sigma_z$, and is expressed as:

$$\tau_w(z) = \rho_w \int_{\sigma_{min}}^{\sigma_z}\int_{-\pi}^{\pi} \beta_g(\sigma,\theta)\sigma^2 N(\sigma,\theta)\frac{k}{k}d\theta d\sigma \tag{11}$$

where $\sigma_z^2 = gk_z\tanh(k_zD)$ and $k_z = \delta/z$; δ is a empirical parameter representing the decay length scale of the wave-induced stress and is set to be 0.03 following Reichl, Hara, and Ginis (2014). Combining Equation (9) and Equation (11), the turbulent stress can be expressed as:

$$\begin{aligned}\tau_t(z) &= \tau_{tot} - \rho_w\int_{\sigma_{min}}^{\sigma_z}\int_{-\pi}^{\pi}\beta_g(\sigma,\theta)\sigma^2N(\sigma,\theta)\tfrac{k}{k}d\theta d\sigma \\ &= \tau_v + \rho_w\int_{\sigma_z}^{\sigma_{max}}\int_{-\pi}^{\pi}\beta_g(\sigma,\theta)\sigma^2N(\sigma,\theta)\tfrac{k}{k}d\theta d\sigma\end{aligned} \tag{12}$$

where σ_{min} and σ_{max} is the minimum and maximum radian frequency of the wave spectrum, respectively. Above the WBL ($z \ge \delta/k_{min}$; $\sigma_z \le \sigma_{min}$), the wave-induced stress $\tau_w(z)$ is zero and the turbulent stress $\tau_t(z)$ is equal to the total wind stress τ_{tot}; while near water surface ($z \le \delta/k_{max}$; $\sigma_z \ge \sigma_{max}$), both $\tau_t(z)$ and $\tau_w(z)$ are constants, with $\tau_w(z = \delta/k_{max})$ represents the total momentum flux absorbed by the surface waves (hereinafter denoted by τ_w), and $\tau_t(z = \delta/k_{max})$ equals to the stress supported by viscosity inside the viscous sublayer τ_v. It is noted that the viscous stress τ_v is the momentum flux directly into the subsurface currents. β_g is the wave growth rate and is give as

$$\beta_g(\sigma,\theta) = C_\beta\sigma\frac{|\tau_t(z)|}{\rho_w c^2}\cos^2(\theta-\theta_\tau) \tag{13}$$

where c is the phase velocity of the relevant wave component; θ_τ is the direction of the turbulent stress; C_β is the Miles constant and set to explicitly account for the effect of swell following Reichl, Hara, and Ginis (2014) (c.f. their Equation 14).

The wave-induced vertical transport rate of energy Π_w is assumed to be mainly from the pressure transport (Hara and Belcher 2004) and thus is equal to the energy flux into the surface waves:

$$\begin{aligned}\Pi_w(z) &= \int_{\sigma_{min}}^{\sigma_z}\tilde{F}_w(\sigma)d\sigma \\ &= \int_{\sigma_{min}}^{\sigma_z}\int_{-\pi}^{\pi}\rho_w\beta_g(\sigma,\theta)g\sigma N(\sigma,\theta)d\theta d\sigma\end{aligned} \tag{14}$$

The viscous dissipation rate is parameterized as:

$$\varepsilon = \frac{[|\tau_t(z)/\rho_a|]^{3/2}}{\kappa z} \tag{15}$$

The wind profile near the sea surface can then be expressed as:

$$\frac{dU}{dz} = \begin{cases} \frac{u_*}{\kappa z}\frac{\tau_{tot}}{|\tau_{tot}|}, & \frac{\delta}{k_{min}} \le z \\ \left[\frac{d\sigma_z}{dz}\tilde{F}_w(\sigma_z) + \frac{\rho_a}{\kappa z}\left|\frac{\tau_t(z)}{\rho_a}\right|^{3/2}\right]\frac{\tau_t(z)}{\tau_t(z)\cdot\tau_{tot}}, & \frac{\delta}{k_{max}} \le z < \frac{\delta}{k_{min}} \\ \left[\frac{\rho_a}{\kappa z}\left|\frac{\tau_v}{\rho_a}\right|^{3/2}\right]\frac{\tau_v}{\tau_v\cdot\tau_{tot}}, & z_v \le z < \frac{\delta}{k_{max}} \end{cases} \tag{16}$$

where z_v is the equivalent roughness scale of the viscous sublayer where the wind speed turns into zero, and is given by

$$z_v = 0.1\frac{\nu_a}{\sqrt{\tau_v/\rho_a}} \tag{17}$$

where ν_a is the air viscosity.

Given the wave spectrum obtained from the wave model and an initial estimate of the total wind stress τ_{tot} from the 10 m wind field, $\tau_w(z)$ and $\tau_t(z)$ at each height (frequency) are calculated by Equation 11–Equation 13), from which the wind profiles can be obtained by integrating Equation 16 from $z = 10$ m to z_v. If the predicted wind speed at z_v is different from zero, the initial estimation of the total stress is adjusted. The above iteration repeats until the final value of the wind speed at the height of z_v converges to zero.

2.4. Momentum flux budget module

Waves absorb energy and momentum from the wind field and in the meantime release it to the ocean. When

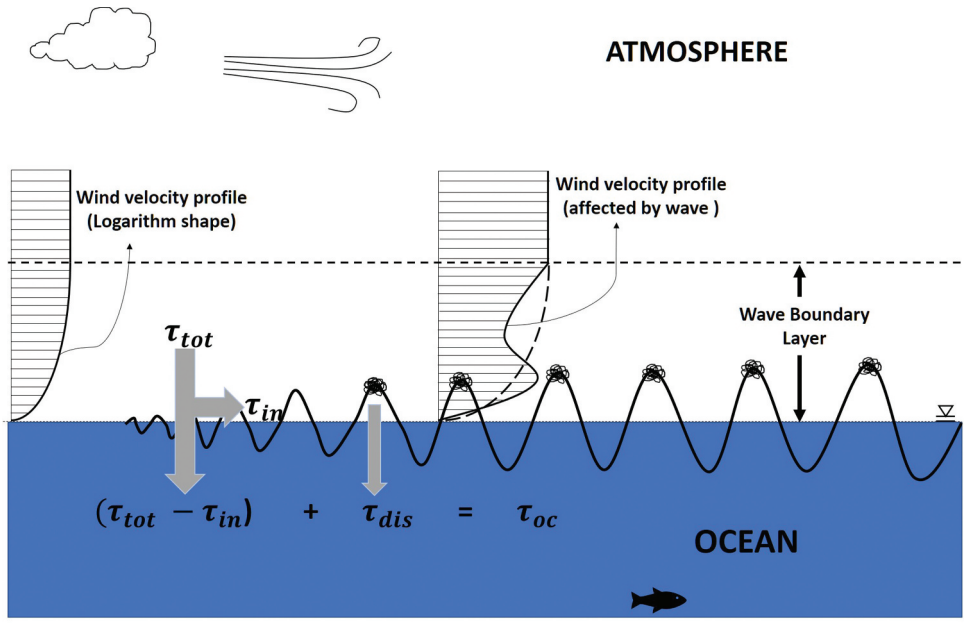

Figure 2. A sketch on the wind stress-wave interaction and conservation of air-sea momentum flux (τ_{tot} and τ_{oc} are the air-side total momentum flux and seaside momentum flux, respectively; τ_{in} and τ_{dis} are the momentum flux absorbed and lost by waves, respectively).

the waves are growing, there is a net momentum influx to the wave field; as the breaking intensifies and the waves become mature, the momentum influx from the atmosphere to the waves tend to close to the flux from the wave field to the ocean; and finally when the waves are decaying, a net momentum out-flux from the wave field will transfer into the ocean (Breivik et al. 2015). Therefore, as shown in Figure 2, the wind-induced stress on the sea surface (i.e. the stress below the oceanic wave field; τ_{oc}) should be equal to the total wind stress (τ_{tot}) taking away the momentum flux absorbed by the wave field (τ_{in}), and adding on the momentum injected from breaking waves to the ocean (τ_{dis}), i.e.

$$\begin{aligned}\tau_{oc} &= \tau_{tot} - \tau_{in} + \tau_{dis} \\ &= \tau_{tot} - \rho_{w0} g \int_0^{\infty} \int_{-\pi}^{\pi} \frac{k}{\sigma} \left[S_{in} - \left(S_{ds,w} + S_{ds,br} + S_{ds,b} \right) \right] d\theta d\sigma \end{aligned} \tag{18}$$

Furthermore, it needs to be noted that when the τ_{dis} is described as a body force (see Section 2.2) in the developed wind stress-wave-ocean coupled model system, the seaside wind stress (i.e. surface stress used in the ocean model) becomes:

$$\mathbf{t_{oc}} = \mathbf{t_{tot}} - \mathbf{t_{in}} \tag{19}$$

3. Numerical tests

To examine the performance of the present model system in producing sea-state-dependent wind stress and investigate the impacts of various wave effects on storm surge and coastal inundation, a series of numerical tests with an idealized ocean basin under the wind fields from idealized TCs were conducted in this study. The ocean domain (Figure 3) covers a rectangular area of 1000 km in the east-west (zonal) direction (i.e. $X = -15 - 985$ km) and 2000 km in the south-north (meridional) direction (i.e. $Y = -1000 - 1000$ km), and is discretised horizontally using an unstructured (triangle) mesh with 2,268,952 nodes and 4,533,186 elements. The mesh resolution is uniformly 100 m in the range of $Y = -204.8 - 204.8$ km and $X = -15 - 36.2$ km, and gradually decreases to 20 km in the north, south and east end of the model domain.

The topography is uniform in the meridional direction, but includes a coastal land surface and a continental shelf in the zonal direction. The land surface has a width of 15 km and a slope of 1:1000; the continental shelf is set with three alternative slope scenarios in this study, i.e. a steep slope of 1:100, a mild slope of 1:500 and a gentle slope of 1:1000. This land and ocean topography configuration is chosen to investigate the role of various wave effects in different bottom slopes, which is based on the representative topography features along the western North Atlantic coast (Wu et al. 2018; Chen, Hara, and Ginis 2020). The wind fields are calculated by a parametric TC approach as described in Zheng et al. (2020) (c.f. its Eqs. (A1) and (A5)), which is adapted from the Holland parametric model (Holland 1980).

Previous studies have showed that the storm surge and coastal inundation are highly sensitive to the storm characteristics (e.g. storm intensity, storm size, translation speed) and coastal topography features

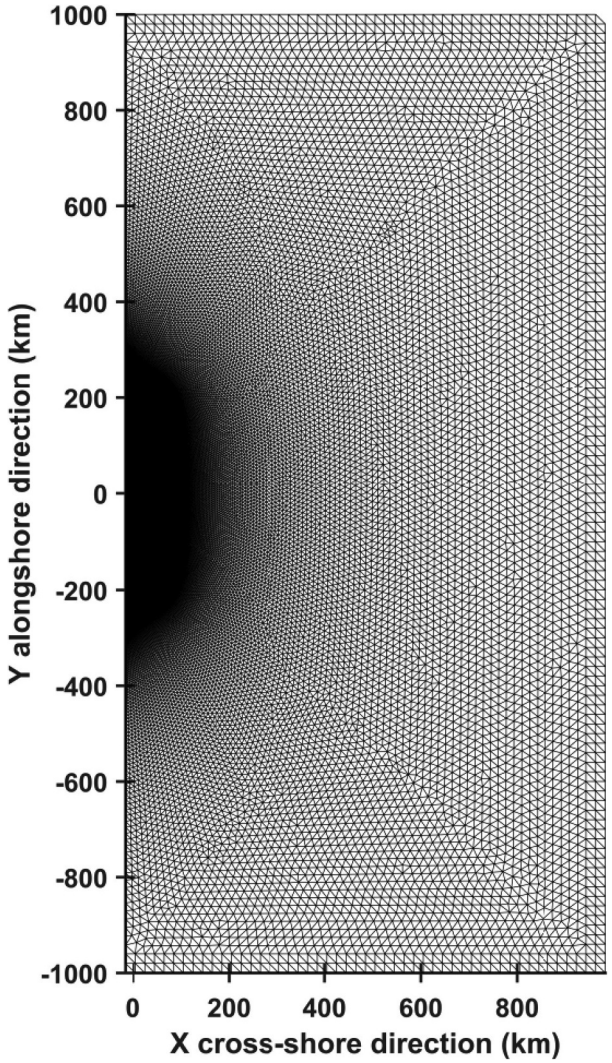

Figure 3. The ocean domain and unstructured grid used by this study.

(Irish, Resio, and Ratcliff 2008; Rego and Chunyan 2009; Wu et al. 2018); the contributions of various wave effects to storm surge and inundation are thus also very likely dependent on these physical parameters. In order to give a more general understanding of the various impacts of wave effects on storm surge and inundation, a total of nine systematic numerical scenarios (Exp_A to Exp_I) are designed by varying one specific parameter from the base scenario (i.e. Exp_A). Exp_A adopts a steep continental shelf slope of 1:100 and a high-intensity, moderate size, fast-moving TC with the maximum wind speed (MWS) of 60 m/s, the radius of maximum wind speed (RMW) of 40 km and the translation speed of 10 m/s. Furthermore, five simulations are conducted for each scenario, each of which represents a specific approach that used to simulate the storm surge and inundation by adopting a different combination of driving forces.[1] Namely, the first simulation (Exp1) only introduces the bulk-HWRF formula calculated wind stress as the only driven forcing[2] but without accounting for any wave effects; based on the E×p1, the second to fourth simulation (i.e. E×p1–4) additionally includes one (i.e. WEC), two (i.e. WEC and WEB) and three (i.e. WEC, WEB and WMWS) aspects of wave effects, respectively. Note that none of above four approaches accounts for the momentum flux balance (MFB) across the air-sea interface; a fifth simulation (Exp5) is therefore conducted to examine the impact of surface momentum flux conservation on the storm surge and inundation modeling. The detailed setup of numerical experiments is summarized in Table 1.

The TCs in all simulations move toward to the coastline along normal direction and travel 48 hours before making landfall, which is long enough for TCs to develop according to Wu et al. (2018). The model results at the time of landfall are used for analysis in the following sections.

4. Results

In this section, results from the five modeling approaches are firstly compared with the base scenario of Exp_A to show their differences. The purpose for this comparison is twofold: one is to review the wave effects of WBA and WEB, and the other more important aim is to investigate the impact of wave-modified surface stress in modeling storm surge and inundation, which is rarely reported in previous studies. In addition, the importance of fully incorporating the three aspects of wave effects (i.e. WBA, WEB and WMWS) and conserving momentum flux across the air-sea interface (MFB) is further examined.

As the storm surge and inundation are highly dependent on the storm characteristics and bathymetry features, it is necessary to investigate the more general role of various wave effects in predicting the accurate surge and inundation under the forcing of TCs with different physical parameters. More sensitivity numerical experiments are thus further conducted and analyzed in the second part of this section.

4.1. The base scenario

4.1.1. Maximum storm surge and maximum inundation distance

Figure 4 shows an example of the comparison of wind stress coefficient (C_d) calculated from the bulk-HWRF formula (solid line) and WBLM (symbols) with increasing 10 m wind speed (U_{10}) from

[1]The logic behind is that each of the above five simulations represents one of the approaches, which was either used historically by former researchers (i.e. E×p1–3) or newly adopted by the present study (i.e. E×p4–5), to predict the storm surge. Therefore, by comparing the results of these five simulations, readers can have intuitive impressions on to what extend the various wave effects have on storm surge or inundation predictions.

[2]The air pressure gradient induced water setup is not investigated in this study.

Table 1. Summary of the numerical test setup.

Scenario	Exp_A*i*[a]	Exp_B*i*	Exp_C*i*	Exp_D*i*	Exp_E*i*
BL	1:100	1:500	1:1000	1:100	1:100
V_T	10 m/s	10 m/s	10 m/s	5 m/s	2.5 m/s
RMW	40 km	40 km	40 km	40 km	40 km
MWS	60 m/s	60 m/s	60 m/s	60 m/s	60 m/s
Scenario	Exp_F*i*	Exp_G*i*	Exp_H*i*	Exp_I*i*	
BL	1:100	1:100	1:100	1:100	
V_T	10 m/s	10 m/s	10 m/s	10 m/s	
RMW	70 km	100 km	40 km	40 km	
MWS	60 m/s	60 m/s	50 m/s	40 m/s	
Test Num	Bulk WS[b]	WBA	WEB	WMWS	MFB
Exp1	✓	×	×	×	×
Exp2	✓	✓	×	×	×
Exp3	✓	✓	✓	×	×
Exp4	×	✓	✓	✓	×
Exp5	×	✓	✓	✓	✓

[a]*i* takes the value of [1–5], represents one of the five simulations in a specific scenario; BL is short for bottom slope; V_T, RMW and MWS represent the translation speed, the radius of maximum wind speed and the maximum wind speed of a TC, respectively.

[b]Bulk WS means that the wind stress is calculated by the bulk-HWRF formula; WBA and WEB represent the wave breaking induced momentum acceleration and wave-enhanced bottom stress, respectively; WMWS is short for the wind stress-wave interaction and is used to represent that the wind stress is calculated by the WBLM method; MFB is used to indicate whether a simulation conserves the momentum flux across the air-sea interface.

the Exp_A5.[3] Comparing with the results of bulk-HWRF formula, the C_d obtained from WBLM shows large variations at a given magnitude of U_{10}, demonstrating the highly dependence of wind stress on the sea-state explicitly. Specially, Chen, Ginis, and Hara (2020); Chen, Hara, and Ginis (2020) showed that the shoaling surface waves in the finite and shallow waters can modify the values of C_d significantly. For example, in the right TC quadrant, the magnitude of C_d can be significantly enhanced compared to its deep water values, indicating its potential to increase storm surge levels and inundation distances. For more detailed descriptions on the wave modified wind stress in deep and finite waters under the TC conditions, readers are referred to Reichl, Hara, and Ginis (2014) and Chen, Ginis, and Hara (2020).

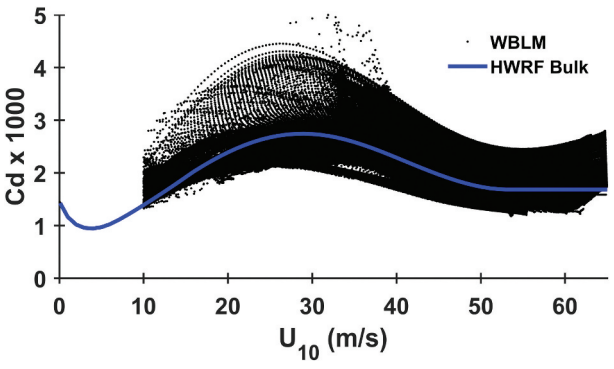

Figure 4. Wind stress coefficient (C_d) versus 10 m wind speed (U_{10}) obtained at all the grid points from Exp_A5 (black points). The blue line represents the bulk-HWRF formula calculated Cd.

[3]Note when U_{10} is smaller than 10 m/s or the significant wave height (H_s) is smaller than 0.5 m, the wind stress is calculated by the bulk-HWRF formula as the WBLM become less reliable in these situations (personal communications with Xuanyu Chen, the author of Chen, Ginis, and Hara (2020)).

A typical example of the simulated storm surge and overland inundation at the landfall time from the same experiment is shown in Figure 5(a); the wind vectors at the same time are also displayed in the background. The wind field shows an asymmetric structure, with larger onshore-directed (lower offshore-directed) wind vector in the right (left) TC quadrant due to the adding (removing) of the TC translation speed. Correspondingly, positive storm surges and prominent overland inundations are observed in the upper part of the model domain, while negative surges in the lower part. The maximum storm surge (i.e. the largest water level at the initial shoreline X = 0.0 km) occurs at a distance of roughly equal to the RMW from the TC center. By contrast, the distance from the maximum inundation location to the TC center is obviously smaller than RMW. This is very likely due to the curvature of wind vector over the land area which has a negative *Y*-component and thus pushes water toward negative *Y* direction overland. The simulated significant wave height (H_s) and wave direction at the same time are shown in Figure 5(b). In the offshore region, the H_s is much higher in the right-front TC quadrant due to the resonance effect induced by the TC propagation (Moon, Ginis, and Hara 2004); while in the nearshore, the H_s is significantly reduced due to depth-induced severe wave breaking. The wave directions are generally aligned with wind directions in the right-rear TC quadrant, but in opposite to or cross with the wind direction in the left-rear quadrant.

Due to the associated tremendous damage in practical engineering applications, the maximum storm surge and maximum inundation distance are often the overriding monitoring indicators during a TC course; thus, they are analyzed primarily in the following sections. The inundation distance is defined as the horizontal distance from the furthest inundated location to the initial shoreline. Table 2 shows the model

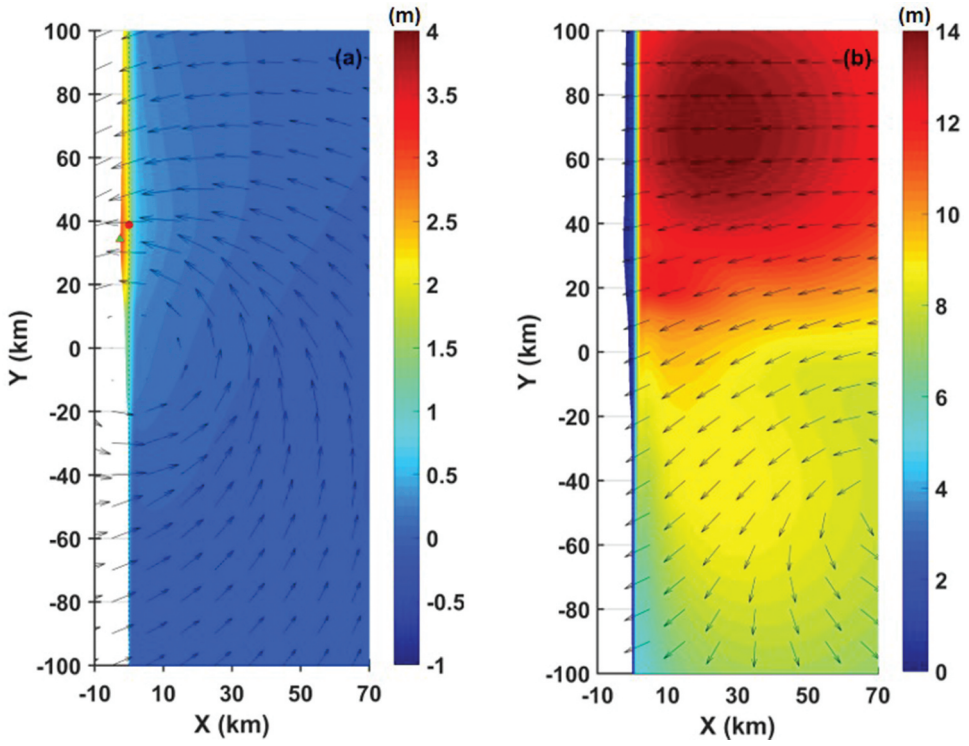

Figure 5. A typical example of model results from Exp_A5 at the time of TC landfall. (a) a snapshot of model predicted storm surge and inundation map (colours) with TC wind field (black arrows); (b) a snapshot of model predicted significant wave height (colours) and mean wave direction (black arrows).

predicted maximum storm surge and inundation distance by the five modeling approaches for the base scenario (i.e. Exp_A1-A5). When wave effects are absent (i.e. Exp_A1), the model predicted a lowest level of maximum storm surge in five simulations. After WBA is accounted for (Exp_A2), the maximum storm surge increases from 0.78 m to 1.75 m with a significant enhancement of 122.78%. By contrast, the maximum storm surge slightly increases (from 1.75 m to 1.77 m) after both the wave effects of WBA and WEB are considered in Exp_A3. Note this positive impact of wave-enhanced bottom stress on storm surge, which may be contrary to one's first expectation, has been reported in previous studies (e.g. Wu et al. 2018). The impacts of WBA and WEB on storm surge are generally in consistent with the previous studies. When the effect of wave modification on wind stress (i.e. WMWS) is included, the maximum storm surge level further increases from 1.77 m to 1.95 m, with an enhancement of 10.2%. This enhancement of storm surge clearly indicates that the wave-modified wind stress has a notable impact on elevating the storm surge levels, which can be important in coastal management and shall be further accounted for in operational storm surge forecasting models. Besides, it shall be noted that most of the previous studies partially emphasized the importance of including wave effects in storm surge modeling, but generally overlooked a fact that the wave growth can also absorb part of wind energy (or wind momentum), subjectively resulting a potential overestimation of the wave effects. Thus to conserve momentum flux across the air-sea interface in the model (see Equation 18) it is important to the accuracy of the prediction. After taking the MFB into account, the resultant maximum storm surge from Exp_A5 decreases as expected. However, the percentage of reduction is only about 3% of the total surge level, suggesting that the conservation of air-sea momentum may not be much important in predicting the storm surges for some specific cases.

The impacts of different wave effects on the inundation distances are also shown in Table 2. Similar to its impact on surge levels, the WBA greatly increases the inundation distance by 900 m (45%). Conversely, the WEB reduces the inundation distance considerably from 2900 m to 2400 m, with a reduction percentage of about 17.2%. This reduction of inundation distance induced by WEB has also been reported in Wu et al. (2018), with possible reasons ascribed to the vertical flow structures over the inundated land. In the following section, the reasons for this reduction is also analyzed by introducing a cross-shore momentum balance analysis. The wave modified wind stress (see model result of Exp_A4) increases the inundation distance by 200 m from 2400 m to 2600 m. Interestingly, the inundation distance obtained from Exp_A5 falls back to 2400 m, indicating the impacts of WMWS and MFB on inundation limit offset with each other. Nevertheless, it shall be noted that both these two effects can change the inundation distance

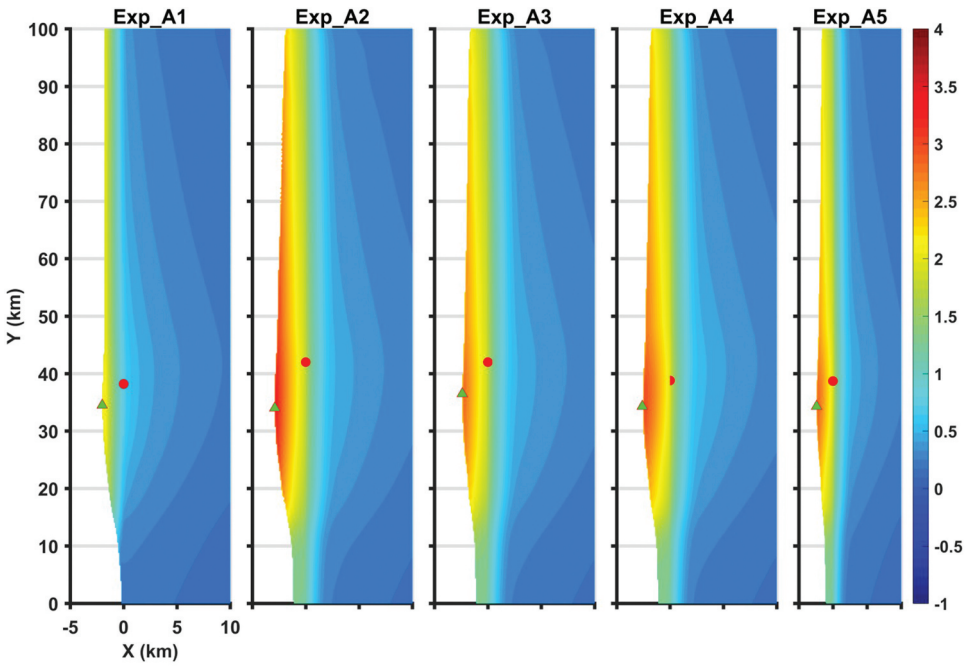

Figure 6. Model predicted storm surge and inundation map from the five simulations of the base scenario Exp_A; red dot and green triangle represent the locations of the predicted maximum storm surge and maximum inundation distance, respectively.

considerably which may complicate the model predictions in practical application with complex topography features and highly varying wind structures and intensities. Comparing with the surge levels, the influence of MFB is more apparent on the inundation distance.

In total, the wave effects can significantly change the storm surge levels and overland inundation distances. Among the three wave aspects, WBA is the most significant factor for both the surge level and inundation distance, while the WMWS contributes in the second role. The percentage of contribution from WBA and WMWS in the total wave-induced surge level (inundation distance) for this particular experiment of Exp_A is about 82.7% (150%) and 15.5% (33.3%), respectively. By contrast, the WEB elevates the surge level slightly but substantially reduces the inundation distance. In addition, these different terms can also affect the location of the maximum surge and inundation as shown in Figure 6 in which the positions of the peak values are presented as the dots and triangles respectively. In these particular results, it is clear that the different combination of wave terms shifts the positions of maximum moderately, within a distance of 5 km alongshore in this specific scenario.

4.1.2. Momentum balance analysis

The impacts of different wave effects are further studied by comparing the depth-integrated cross-shore momentum balance patterns obtained from the Exp_A1-A4 (Figure 7) in this section. When no wave effect is included (see Figure 7(a)), the cross-shore momentum terms are mainly balanced between the onshore-directed (negative) wind stress, Coriolis force and the offshore-directed (positive) pressure gradient force in a quasi-steady state (i.e. the time derivative term $\frac{\partial V}{\partial t}$ in Equation 3 is close to zero) in the sea area (X $>$ 0 km). By contrast in the land area the bottom friction, which is onshore-directed with a negligible magnitude in the sea area, becomes significant and offshore-directed due to the shallow water depth and

Table 2. Model calculated maximum storm surge and maximum inundation distance from the base scenario (Exp_a1-A5).

Experiments	Exp_A1	Exp_A2	Exp_A3	Exp_A4	Exp_A5
MSS (m)*	0.79	1.75	1.77	1.95	1.89
Relative Change1	\	122.78%	0.57%	10.17%	−3.08%
Relative Change2	41.80%	51.32%	0.53%	9.52%	−3.17%
MID (m)*	2000	2900	2400	2600	2400
Relative Change1	\	45%	−17.24%	8.33%	−7.69%
Relative Change2	83.33%	37.5%	−20.83%	8.33%	−8.33%

* MSS and MID are short for the maximum storm surge and maximum inundation distance, respectively. The"Relative Change1" values represent the change of MSS (MID) of the present experiment Exp_Ai relative to the previous one Exp_A($i-1$), and are calculated by the formula of $\frac{Exp\_A(i)-Exp\_A(i-1)}{Exp\_A(i-1)} * 100\%$; while "Relative Change2" represent the ratio of the MSS or MID changes to the total storm surge or total inundation distance calculated from the Exp_A5.

Table 3. Model calculated maximum storm surge and maximum inundation distance from the experiment scenarios with varying bottom slopes (Exp_a, Exp_B, Exp_C).

	Exps (Scenario)	Exp_*x*1	Exp_*x*2	Exp_*x*3	Exp_*x*4	Exp_*x*5
MSS (m)	Exp_A	0.79	1.76	1.77	1.95	1.89
	{BL = 1:100}	\	122.78%	0.57%	10.17%	−3.08%
		41.80%	51.32%	0.53%	9.52%	−3.17%
&	Exp_B	2.46	3.25	3.24	3.70	3.47
Relative Changes	{BL = 1:500}	\	32.11%	−0.31%	14.19%	−6.21%
		70.89%	22.77%	−0.29%	13.26%	−6.63%
	Exp_C	3.64	4.49	4.43	4.89	4.49
	{BL = 1:1000}	\	23.35%	−1.34%	10.38%	−8.18%
		81.07%	18.93%	−1.34%	10.25%	−8.91%
MID (m)	Exp_A	2000	2900	2400	2600	2400
		\	45%	−17.24%	8.33%	−7.69%
		83.33%	37.5%	−20.83%	8.33%	−8.33%
&	Exp_B	3300	4100	3600	3800	3400
Relative Changes		\	24.24%	−12.20%	5.56%	−10.53%
		97.06%	23.53%	−14.71%	5.88%	−11.76%
	Exp_C	4100	5000	4500	4800	4100
		\	21.95%	−10.0%	6.67%	−14.58%
		100.00%	21.95%	−12.20%	7.32%	−17.07%

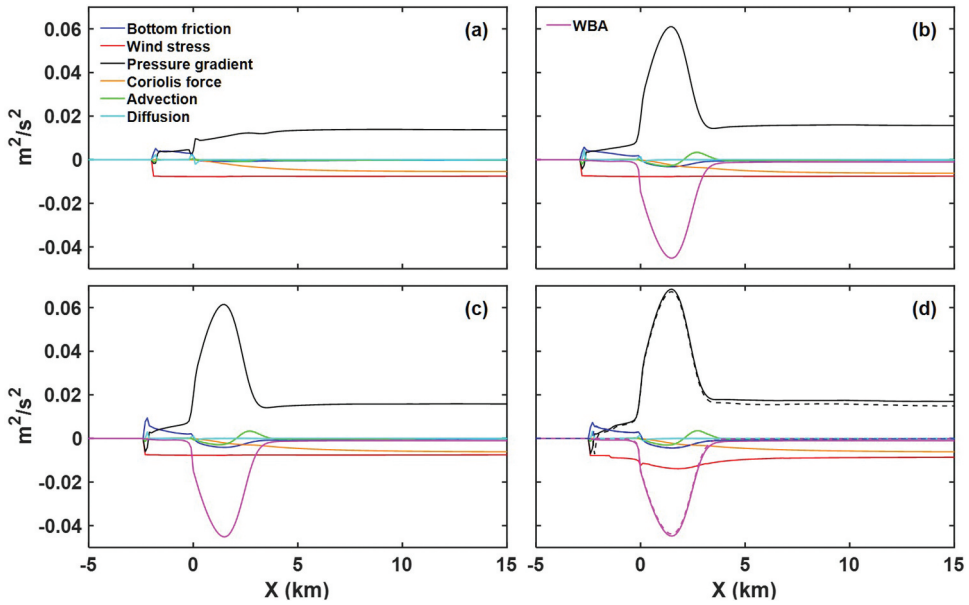

Figure 7. Leading terms of the depth-integrated cross-shore momentum balance equation at the location of Y = 40 km when the TC makes landfall. The solid lines in (a)-(d) are results from Exp_A1-A4, respectively; the dashed lines in (d) are from Exp_A5.

Table 4. Same with Table 3 but for experiment scenarios with varying TC translation speed (Exp_a, Exp_D, Exp_E).

	Exps (Scenario)	Exp_x1	Exp_x2	Exp_x3	Exp_x4	Exp_x5
MSS (m)	Exp_A	0.79	1.76	1.77	1.95	1.89
	{V_T=10 m/s}	\	122.78%	0.57%	10.17%	−3.08%
		41.80%	51.32%	0.53%	9.52%	−3.17%
&	Exp_D	0.79	1.57	1.58	1.73	1.66
Relative Changes	{V_T=5 m/s}	\	98.73%	0.64%	9.49%	−4.05%
		47.59%	46.99%	0.60%	9.04%	−4.22%
	Exp_E	0.76	1.36	1.37	1.48	1.41
	{V_T=2.5 m/s}	\	78.95%	0.74%	8.03%	−4.73%
		53.90%	42.55%	0.71%	7.80%	−4.96%
MID (m)	Exp_A	2000	2900	2400	2600	2400
		\	45%	−17.24%	8.33%	−7.69%
		83.33%	37.5%	−20.83%	8.33%	−8.33%
&	Exp_D	3300	3600	2800	3000	2700
Relative Changes		\	9.09%	−22.22%	7.14%	−10.00%
		122.33%	11.11%	−29.63%	7.41%	−11.11%
	Exp_E	5700	4500	3100	3300	2900
		\	−21.05%	−31.11%	6.45%	−12.12%
		196.55%	−41.38%	−48.28%	6.90%	−13.79%

the changed bottom flow direction. The pressure gradient force hence reduces correspondingly in order to, together with the enhanced bottom friction, balance the nearly uniform wind stress. After the wave effect of WBA is considered (Figure 7(b)), the onshore momentum is greatly enhanced in the surf zone and lower land area due to the wave-breaking induced onshore momentum acceleration. As a result, the offshore-directed pressure gradient force significantly increases to counteract this newly introduced onshore term, which hence greatly elevates the maximum storm surge level and extends the maximum inundation distance. The imbalance of the vertical uniform pressure gradient force and vertical varying WBA promotes the development of the offshore-directed undertow, which induces a larger onshore-directed bottom friction; the magnitude of advection term also increases considerably due to the local convergence/divergence of currents. Further onshore in the upper land area, the pressure gradient force decreases gradually corresponding to the small magnitude of WBA but with a magnitude still larger than that show in Figure 7(a) mainly due to the gradually enhanced bottom friction; offshore from the surf zone (X > 4 km) the momentum balance pattern is not changed. Similar cross-shore momentum balance patterns are observed in Figure 7(c) when the wave effect of WEB is further taken into account. A close examination of the difference between Figures 7(b) and 7(c) reveals that waves enhance the magnitude of bottom friction considerably in the surf zone and land area, which is totally offset by the change of pressure gradient force. As a result, the maximum storm surge (inundation distance) is slightly elevated (much reduced) by the enhancement (reduction) of the pressure gradient force in the surf zone (land area) as shown in Table 2. Similar patterns of cross-shore momentum balance as above are also reported in Wu et al. (2018), which highlights the complex hydrodynamic behaviors in the sea and land areas under a TC condition.

As shown in Figure 7(d), the sea-state-dependent wind stress increases considerably in the shoaling region and surf zone due to the wave modification effect. The pressure gradient force increases significantly to counteract this effect and hence the maximum storm surge and inundation distance are also increased (see Table 2). Similarly, when the momentum flux across the air-sea interface is conserved in the model, the pressure gradient force and hence the maximum storm surge and inundation distance decrease as the wave absorbed part of onshore momentum flux (i.e. τ_{in}) is excluded from the model. Overall, the momentum balance patterns shown in Figure 7(b–d) clearly reveal the impacts of various wave effects on cross-shore momentum balance. The inclusion of one or more wave effects in the momentum equation is primarily counteracted by the change of pressure gradient force, which hence results in the increase or decrease of the storm surge level and inundation distance.

4.2. More general scenarios

Table 3 compares the calculated maximum storm surge and maximum inundation distance from the experiment scenarios with varying bottom slopes (i.e. Exp_A, Exp_B and Exp_C). The maximum storm surge increases as the bottom slope decreases, no matter the wave effects are taken into account or not. The WBA has a positive effect on the storm surge. However, its contribution to the total storm surge (i.e. the model results from Exp5) abruptly decreases after the bottom slope decreases from 1:100 to 1:500 and continues to decrease at the bottom slope of 1:1000. By contrast, WEB has a weak positive contribution at the steep bottom slope of 1:100 and a weak negative contribution at the moderate bottom slope of 1:500. This weak negative contribution further enhances with decreasing bottom slope. The proportion of surge level due to WMWS generally stays above 10%. Recalling the

Table 5. Same with Table 3 but for experiment scenarios with varying radius of maximum wind speed (Exp_a, Exp_F, Exp_G).

	Exps (Scenario)	Exp_x1	Exp_x2	Exp_x3	Exp_x4	Exp_x5
MSS (m)	Exp_A	0.79	1.76	1.77	1.95	1.89
	{RMW=40 km}	\	122.78%	0.57%	10.17%	−3.08%
		41.80%	51.32%	0.53%	9.52%	−3.17%
&	Exp_F	0.85	1.97	1.98	2.18	2.11
Relative Changes	{RMW=70 km}	\	131.76%	0.51%	10.10%	−3.21%
		40.28%	53.08%	0.47%	9.48%	−3.32%
	Exp_G	0.89	2.10	2.11	2.32	2.25
	{RMW=100 km}	\	135.96%	0.48%	9.95%	−3.02%
		39.56%	53.78%	0.44%	9.33%	−3.11%
MID (m)	Exp_A	2000	2900	2400	2600	2400
		\	45%	−17.24%	8.33%	−7.69%
		83.33%	37.5%	−20.83%	8.33%	−8.33%
&	Exp_F	3200	4000	3300	3500	3300
Relative Changes		\	25.00%	−17.50%	6.06%	−5.71%
		96.97%	24.24%	−21.21%	6.06%	−6.06%
	Exp_G	4400	5000	3900	4200	4000
		\	13.64%	−22.00%	7.69%	−4.76%
		110.00%	15.00%	−27.50%	7.50%	−5.00%

Table 6. Same with Table 3 but for experiment scenarios with varying maximum wind speed (Exp_a, Exp_H, Exp_I).

	Exps (Scenario)	Exp_x1	Exp_x2	Exp_x3	Exp_x4	Exp_x5
MSS (m)	Exp_A	0.79	1.76	1.77	1.95	1.89
	{MWS=60 m/s}	\	122.78%	0.57%	10.17%	−3.08%
		41.80%	51.32%	0.53%	9.52%	−3.17%
&	Exp_H	0.67	1.81	1.82	1.92	1.82
Relative Changes	{MWS=50 m/s}	\	170.15%	0.55%	5.49%	−5.21%
		26.81%	62.64%	0.55%	5.49%	−5.49%
	Exp_I	0.61	1.69	1.70	1.78	1.69
	{MWS=40 m/s}	\	177.05%	0.59%	4.71%	−5.06%
		36.09%	63.91%	0.59%	4.73%	−5.33%
MID (m)	Exp_A	2000	2900	2400	2600	2400
		\	45%	−17.24%	8.33%	−7.69%
		83.33%	37.5%	−20.83%	8.33%	−8.33%
&	Exp_H	1600	2600	2200	2300	2100
Relative Changes		\	62.50%	−15.38%	4.55%	−8.70%
		76.19%	47.62%	−19.05%	4.76%	−9.52%
	Exp_I	1400	2300	1900	2000	1800
		\	64.29%	−17.39%	5.26%	−10.00%
		77.78%	50.00%	−22.22%	5.56%	−11.11%

increasingly reduced role of WBA, the effect of WMWS is thus more important in cases with small bottom slopes. Ignoring this process can greatly underestimate the total wave effects in contributing to the peak storm surge. The percentage of declined surge resulted from MFB gradually enhances as the bottom slope decreases, implying that the storm surge levels are more likely to be overestimated in areas with small bottom slope in previous studies. Similar findings can be obtained when analyzing the contributions of different wave effects to the maximum inundation distance in situations with varying bottom slopes. However, it is noted that the WEB always retards the extension of inundation, while the magnitude of reduced distance is not sensitive to the bottom slopes.

The variations of maximum storm surge and maximum inundation distance with changing TC translation speed (V_T) are shown in Table 4. The increasing translation speed can enhance the wind speed in the right TC quadrant and thus has a potential to elevate the maximum storm surge levels. In the meantime, the faster-moving TC reduces the duration that TC wind fields acting on the water body. The final wind stress-induced surge level (model results from E×p1) is thus a result of these two contradictory effects, which saturate at $V_T = 10$ m/s. However, after considering the wave effects the surge level monotonically increases as V_T increases from 2.5 m/s to 10 m/s. This is attribute to the larger wave height and more pronounced wave-breaking induced dissipation energy associated with a faster-moving TC. Note that Wu et al. (2018) once reported a critical translation speed of about 14 m/s, above which the total surge height decreases gradually. The enhanced surge level due to WMWS gradually increases with increasing TC translation speed (from 0.11 m to 0.18 m). Its proportion in the total surge height (i.e. the model results from E×p5) is above 7.8% and slightly increases from 7.8% at $V_T = 2.5$ m/s to 9.52% at $V_T = 10$ m/s, indicating the universal importance of the impact of WMWS on storm surge levels which are not sensitive to the TC translation speed. Similarly, the reduced surge height due to MFB is generally within 5% of the total surge height which also shows a weak dependence on the TC translation speed. Contrary to the maximum surge level, the maximum inundation distance reduces greatly with increasing translation speed, no matter with or without the various wave effects. Similar results have also been reported in some previous studies (e.g. Rego and Chunyan 2009; Wu et al. 2018), with the primary possible reason ascribed to the shorter wind duration that a faster TC occupies to push the water inland. Nevertheless, it is noted that the contribution from WBA increases gradually, while the negative contribution from WEB considerably reduces, with the increasing V_T. The impact of WMWS on inundation is similar with its impact on surge level; by contrast the momentum flux conservation shows its greater importance in a slower-moving TC.

It is known that a larger TC[4] produces higher storm surges and inundation distances. The results in Table 5 show that the bulk wind stress induced surge level moderately increases from 0.79 m at RMW = 40 km to 0.89 m at RMW = 100 km, while its proportion in total surge reduces from 41.80% to 39.56% on the contrary. By contrast, both the WBA-induced contribution to surge level and its proportion in the total surge height increase moderately. However, it is interesting to note that the sum up of WBA and bulk wind stress-induced surge basically contributes to about 93% of the total surge height, regardless of the TC size. Correspondingly, the proportions of surge level in total surge height resulted from the WEB, WMWS, and MFB basically keep the same value, indicating that they are all have a weak dependence on TC

[4]In this study, we use the radius of maximum wind speed to represent a TC size.

sizes. Specifically, the WMWS can elevate about 9.5% of the total surge height and thus shall not be ignored in models. Compared with the storm surge, the maximum inundation distance is much more sensitive to the TC sizes. Table 5 shows that a larger TC can greatly increase the inundation limit for all cases no matter with or without the wave effects. The positive effect of WBA on inundation distance decreases gradually with increasing TC sizes, in terms of both its contribution and proportion in the total inundation distance. While the negative effect of WEB increases steadily. By contrast, the enhanced inundation distance due to WMWS is less sensitive to TC size, with its proportion in the total inundation distance staying roughly around 7%. Summing up the WBA, WEB, and WMWS induced proportion shows that the total positive wave effect declines as TC size increases, from which perspective the sole role of WMWS is increasingly important in a larger TC. The negative effect of MFB on inundation gradually decreases with increasing TC sizes.

Table 6 shows the variations of maximum storm surge with changing TC intensity. As the TC intensity increases, the proportion of WBA-induced wave setup in the total surge gradually decreases, indicating a more essential role of WBA for a weaker TC in predicting the peak storm surge. Conversely, the impact of WMWS in the total surge steadily increases with an enhanced TC intensity, suggesting an increasing need to include this effect in storm surge modeling for a stronger TC. As a result, the including of WMWS makes the total wave impact on surge levels decrease with the TC intensity at a more gentle rate. In addition, it is noted that the magnitude of WBA-induced wave setup reduces moderately from 1.14 m at MWS = 50 m/s to 0.97 m at MWS = 60 m/s. Similar results are also observed in the study of Wu et al. (2018). The exact reason is still unknown, but it is very likely due to the misalignment between wave (thus the direction of WBA) and wind directions. Accounting for the momentum flux conservation reduces the surge level by about 5%, which changes little with TC intensity. As the TC intensity increases, the responses of maximum inundation distance to the three wave effects are similar with that of the maximum storm surge. However, the maximum inundation distance shows more dependence on the momentum flux conservation, the magnitude of which reduces more significantly in a weaker TC.

As comparison to above TC conditions, a series of numerical tests with uniform and constant wind were also conducted. Similar model domain setups as described in previous section were used. Overall, the model results show consistent findings with those obtained from TC scenarios. In particular, the WBA contributes most to the peak storm surge, the WMWS contributes in the second role and the WEB can moderately elevate the storm surge height. Their impacts to the inundation limit show slightly complex variations than that in the TC conditions, although the extreme conditions used in the test, e.g. wind speed of 60 m/s, remain as largely hypothetical. The detailed results analysis and discussion are included in Appendix A.

5. Summary

In this study, we extend a three-dimensional wave-ocean coupled model (Zheng et al. 2017) into the wind stress-wave-ocean coupled coastal model system, with a new wave boundary layer model (WBLM) to account for the wind stress-wave interactions and including a flux budget module to guarantee the conservation of momentum flux across the air-sea interface.

The developed model system is applied into sets of idealized numerical tests with a simplified model domain under the forcing of idealized landfalling tropical cyclones (TCs) with various TC characteristics. A base scenario is firstly designed to study the impact of three wave effects and the momentum flux conservation across air-sea interface on the storm surge and coastal inundation modeling, which adopts a steep continental shelf slope of 1:100 and a high-intensity, moderate size, fast-moving TC with the maximum wind speed (MWS) of 60 m/s, radius of maximum wind speed (RMW) of 40 km and translation speed of 10 m/s. The comparison of model results from five model approaches from this base scenario suggests that the wave modified wind stress (WMWS) can considerably elevate the maximum storm surge and extend the maximum inundation limit, and thus shall be included in future operational storm surge forecasting models. By contrast, without accounting for the momentum flux conservation (MFB), the previous models are very likely to have overestimated the distances of inundation.

Further analysis are conducted by systematically generalizing the base scenario into scenarios with different TC characteristics (i.e. TC intensity, TC size and TC translation speed) and topography features. The present study confirms previous findings on the role of wave-breaking induced acceleration (WBA) and wave-enhanced bottom friction (WEB) in modeling storm surge and coastal inundation under different physical parameters. Major conclusions are summarized as follows:

(1) The WBA contributes most in three wave effects to the peak storm surge at the initial shoreline and the inundation distance. Its proportion in the total surge height increases considerably with the increasing of bottom slope, TC translation speed (V_T) or TC size, but decreases with increasing TC intensity.
(2) The contribution of WBA to maximum inundation distance is similar with its contribution to

surge, except that its proportion in total inundation declines greatly as the TC size increases.

(3) The WEB can elevate the surge levels in scenarios with steep bottom slope, regardless of the TC characteristics.

(4) By contrast, the maximum inundation distance is always greatly reduced by the WEB; its reduction degree enhances with increasing of the bottom slope or TC size, but declines as V_T increases. More importantly, this study investigates the impact of WMWS and MFB on the storm surge and inundation predictions, which are generally ignored in previous studies. The model results indicate that:

(5) The WMWS induced surge accounts for 9%–13% of the total surge height in a relatively high-intensity TC (MWS = 60 m/s), and its contribution is not sensitive to the bottom slope, TC size, and TC translation speed. As the TC intensity decreases, the effect of WMWS decreases slightly, but its proportion still remains around 5%. Ignoring this effect can thus significantly (considerably) underestimate the peak surge level in high- (moderate-) intensity TCs.

(6) Similarly, the WMWS can moderately extend the inundation distance by 5%–8%, which also depends weakly on the TC characteristics.

(7) After taking account of the MFB, the storm surge at the initial shoreline decreases by 3%–5% with varying TC characteristics. The degree of MFB-induced surge reduction enhances as bottom slope decreases and can be up to 9% at the bottom slope of 1:1000.

(8) The effect of MFB on inundation is similar to its effect on storm surge, but its degree of reduction is more significant.

Acknowledgments

PZ thanks Dr. Xuanyu Chen for the constructive discussions. The authors thank the National Supercomputing Centre in Jinan for the provided computational support.

Disclosure statement

No potential conflict of interest was reported by the authors.

Funding

This research was jointly sponsored by the National Key R&D Program of China (2022YFE 0113500), National Natural Science Foundation of China (No. 42006154, No. 41906028), Basic Scientific Fund for National Public Research Institutes of China (2019Q06) and the National Key R&D Program of China (2022YFC 3104400). This research was also partly supported by the Engineering and Physical Science Research Council (United Kingdom, No. EP/R024537/1), National Natural Science Foundation of China (China, No. 51761135022) and Dutch Research Council (NWO, the Netherlands, No. ALWSD.2016.026) jointly funded ANCODE project.

References

Babanin, Alexander V, and Vladimir K Makin. 2008. "Effects of Wind Trend and Gustiness on the Sea Drag: Lake George Study." *Journal of Geophysical Research: Oceans* 113 (C2): . doi:10.1029/2007JC004233.

Babanin, Alexander V, Miguel Onorato, and Fangli Qiao. 2012. "Surface Waves and Wave-Coupled Effects in Lower Atmosphere and Upper Ocean." *Journal of Geophysical Research: Oceans* 117 (C11). doi:10.1029/2012JC007932.

Biswas, Mrinal K, Sergio Abarca, Ligia Bernardet, Isaac Ginis, Evelyn Grell, Michael Iacono, Evan Kalina, et al. 2018. "Hurricane Weather Research and Forecasting (HWRF) Model: 2018 Scientific Documentation." https://dtcenter.org/community-code/hurricane-wrf-hwrf/documentation

Breivik, Øyvind, Kristian Mogensen, Jean-Raymond Bidlot, Magdalena Alonso Balmaseda, and Peter AEM Janssen. 2015. "Surface Wave Effects in the NEMO Ocean Model: Forced and Coupled Experiments." *Journal of Geophysical Research: Oceans* 120 (4): 2973–2992. doi:10.1002/2014JC010565.

Charnock, H. 1955. "Wind Stress on a Water Surface." *Quarterly Journal of the Royal Meteorological Society* 81 (350): 639–640. doi:10.1002/qj.49708135027.

Chen, Xuanyu, Isaac Ginis, and Tetsu Hara. 2020. "Impact of Shoaling Ocean Surface Waves on Wind Stress and Drag Coefficient in Coastal Waters: 2. Tropical Cyclones." *Journal of Geophysical Research: Oceans* 125 (7): e2020JC016223. doi:10.1029/2020JC016223.

Chen, Xuanyu, Tetsu Hara, and Isaac Ginis. 2020. "Impact of Shoaling Ocean Surface Waves on Wind Stress and Drag Coefficient in Coastal Waters: 1. Uniform Wind." *Journal of Geophysical Research: Oceans* 125 (7): e2020JC016222. doi:10.1029/2020JC016222.

Chen, Changsheng, Hedong Liu, and Robert C. Beardsley. 2003. "An Unstructured Grid, Finite-Volume, Three-Dimensional, Primitive Equations Ocean Model: Application to Coastal Ocean and Estuaries." *Journal of Atmospheric and Oceanic Technology* 20 (1): 159–186. doi:10.1175/1520-0426(2003)020<0159:AUGFVT>2.0.CO;2.

Chen, Yingjian, and Yu. Xiping. 2016. "Enhancement of Wind Stress Evaluation Method Under Storm Conditions." *Climate Dynamics* 47 (12): 3833–3843. doi:10.1007/s00382-016-3044-4.

Chen, Yingjian, and Yu. Xiping. 2017. "Sensitivity of Storm Wave Modeling to Wind Stress Evaluation Methods." *Journal of Advances in Modeling Earth Systems* 9 (2): 893–907. doi:10.1002/2016MS000850.

De Dominicis, Michela, Judith Wolf, Svetlana Jevrejeva, Peng Zheng, and Zhan Hu. 2020. "Future Interactions Between Sea Level Rise, Tides, and Storm Surges in the World's Largest Urban Area." *Geophysical Research Letters* 47 (4): e2020GL087002. doi:10.1029/2020GL087002.

Dietrich, J Casey, S. Tanaka, Joannes J Westerink, Clinton N Dawson, RA. Luettich, Marcel Zijlema, Leo H Holthuijsen, JM. Smith, LG. Westerink, and HJ. Westerink. 2012. "Performance of the Unstructured-Mesh, SWAN+ ADCIRC Model in Computing Hurricane Waves and Surge." *Journal of Scientific Computing* 52 (2): 468–497. doi:10.1007/s10915-011-9555-6.

Donelan, Mark A, Fred W Dobson, Stuart D Smith, and Robert J Anderson. 1993. "On the Dependence of Sea Surface Roughness on Wave Development." *Journal of Physical*

Oceanography 23 (9): 2143–2149. doi:10.1175/1520-0485(1993)023<2143:OTDOSS>2.0.CO;2.

Drennan, William M, Peter K Taylor, and Margaret J Yelland. 2005. "Parameterizing the Sea Surface Roughness." *Journal of Physical Oceanography* 35 (5): 835–848. doi:10.1175/JPO2704.1.

Du, Jianting, Rodolfo Bolaños, and Xiaoli Guo Larsén. 2017. "The Use of a Wave Boundary Layer Model in SWAN." *Journal of Geophysical Research: Oceans* 122 (1): 42–62. doi:10.1002/2016JC012104.

Hara, Tetsu, and Stephen E Belcher. 2004. "Wind Profile and Drag Coefficient Over Mature Ocean Surface Wave Spectra." *Journal of Physical Oceanography* 34 (11): 2345–2358. doi:10.1175/JPO2633.1.

Holland, Greg J. 1980. "An Analytic Model of the Wind and Pressure Profiles in Hurricanes." *Monthly Weather Review* 108 (8): 1212–1218. doi:10.1175/1520-0493(1980)108<1212:AAMOTW>2.0.CO;2.

Irish, Jennifer L, Donald T Resio, and Jay J Ratcliff. 2008. "The Influence of Storm Size on Hurricane Surge." *Journal of Physical Oceanography* 38 (9): 2003–2013. doi:10.1175/2008JPO3727.1.

Janssen, Peter AEM. 2012. "Ocean Wave Effects on the Daily Cycle in SST." *Journal of Geophysical Research: Oceans* 117 (C11). doi:10.1029/2012JC007943.

Jianting, Du, Rodolfo Bolaños, Xiaoli Guo Larsén, and Mark C Kelly. 2019. "Wave Boundary Layer Model in SWAN Revisited." *Ocean Science* 15 (2): 361–377. doi:10.5194/os-15-361-2019.

Large, WG., and S. Pond. 1981. "Open Ocean Momentum Flux Measurements in Moderate to Strong Winds." *Journal of Physical Oceanography* 11 (3): 324–336. doi:10.1175/1520-0485(1981)011<0324:OOMFMI>2.0.CO;2.

Mao, Miaohua, and Meng Xia. 2017. "Dynamics of Wave–Current–Surge Interactions in Lake Michigan: A Model Comparison." *Ocean Modelling* 110: 1–20. doi:10.1016/j.ocemod.2016.12.007.

McWilliams, James C., Juan M. Restrepo, and Emily M. Lane. 2004. "An Asymptotic Theory for the Interaction of Waves and Currents in Coastal Waters." *Journal of Fluid Mechanics* 511: 135C178. doi:10.1017/S0022112004009358.

Monin, Andreĭ Sergeevich, and Aleksandr Mikhalovich Obukhov. 1954. "Basic Laws of Turbulent Mixing in the Surface Layer of the Atmosphere." *Contributions of the Geophysical Institute of the Academy of Sciences USSR* 151 (163): e187.

Moon, IL-JU., Isaac Ginis, and Tetsu Hara. 2004. "Effect of Surface Waves on Air–Sea Momentum Exchange. Part II: Behavior of Drag Coefficient Under Tropical Cyclones." *Journal of the Atmospheric Sciences* 61 (19): 2334–2348. doi:10.1175/1520-0469(2004)061<2334:EOSWOA>2.0.CO;2.

Moon, Il-Ju, Jae-Il Kwon, Jong-Chan Lee, Jae-Seol Shim, Sok Kuh Kang, Seok Jae Kwon, and S J. Kwon. 2009. "Effect of the Surface Wind Stress Parameterization on the Storm Surge Modeling." *Ocean Modelling* 29 (2): 115–127. doi:10.1016/j.ocemod.2009.03.006.

Rego, Joao Lima, and Li. Chunyan. 2009. "On the Importance of the Forward Speed of Hurricanes in Storm Surge Forecasting: A Numerical Study." *Geophysical Research Letters* 36 (7). doi:10.1029/2008GL036953.

Reichl, Brandon G, Tetsu Hara, and Isaac Ginis. 2014. "Sea State Dependence of the Wind Stress Over the Ocean Under Hurricane Winds." *Journal of Geophysical Research: Oceans* 119 (1): 30–51. doi:10.1002/2013JC009289.

Reniers, A.J.H.M., E.B. Thornton, T.P. Stanton, and J.A. Roelvink. 2004. "Vertical Flow Structure During Sandy Duck: Observations and Modeling." *Coastal Engineering* 51 (3): 237–260. doi:10.1016/j.coastaleng.2004.02.001.

The SWAN Team. 2018. *SWAN Scientific and Technical Documentation: SWAN Cycle III Version 41.20A*. Delft, The Netherlands: Delft University of Technology.

Taylor, Peter K, and Margaret J Yelland. 2001. "The Dependence of Sea Surface Roughness on the Height and Steepness of the Waves." *Journal of Physical Oceanography* 31 (2): 572–590. doi:10.1175/1520-0485(2001)031<0572:TDOSSR>2.0.CO;2.

Uchiyama, Yusuke, James C. McWilliams, and Alexander F. Shchepetkin. 2010. "Wave-Current Interaction in an Oceanic Circulation Model with a Vortex-Force Formalism: Application to the Surf Zone." *Ocean Modelling* 34 (1): 16–35. doi:10.1016/j.ocemod.2010.04.002.

Wang, Pengcheng, and Jinyu Sheng. 2016. "A Comparative Study of Wave-Current Interactions Over the Eastern Canadian Shelf Under Severe Weather Conditions Using a Coupled Wave-Circulation Model." *Journal of Geophysical Research: Oceans* 121 (7): 5252–5281. doi:10.1002/2016JC011758.

Wu, Jin. 1982. "Wind-Stress Coefficients Over Sea Surface from Breeze to Hurricane." *Journal of Geophysical Research: Oceans* 87 (C12): 9704–9706. doi:10.1029/JC087iC12p09704.

Wu, Guoxiang, Fengyan Shi, James T Kirby, Bingchen Liang, and Jian Shi. 2018. "Modeling Wave Effects on Storm Surge and Coastal Inundation." *Coastal Engineering* 140: 371–382. doi:10.1016/j.coastaleng.2018.08.011.

Zheng, Peng, Li Ming, Joep van der Zanden, Judith Wolf, Xueen Chen, and Caixia Wang. 2017. "A 3D Unstructured Grid Nearshore Hydrodynamic Model Based on the Vortex Force Formalism." *Ocean Modelling* 116: 48–69. doi:10.1016/j.ocemod.2017.06.003.

Zheng, Peng, Li Ming, Caixia Wang, Judith Wolf, Xueen Chen, Michela De Dominicis, Peng Yao, and Hu. Zhan. 2020. "Tide-Surge Interaction in the Pearl River Estuary: A Case Study of Typhoon Hato." *Frontiers in Marine Science* 7: 236. doi:10.3389/fmars.2020.00236.

Zheng, Peng, Li Ming, Caixia Wang, Judith Wolf, Ping Dong, Xueen Chen, Peng Yao, Michela De Dominicis, and Hu. Zhan. submitted. "Wave-Current-Surge Interaction in the Pearl River Estuary During Typhoon Hato." *Journal of Geophysical Research: Oceans* 279:108138

Zijlema, M. 2010. "Computation of Wind-Wave Spectra in Coastal Waters with SWAN on Unstructured Grids." *Coastal Engineering* 57 (3): 267–277. doi:10.1016/j.coastaleng.2009.10.011.

Appendix

Appendix A. Constant uniform wind scenarios

In addition to the TC conditions, in this section the impacts of wave effects on storm surge and inundation under uniform constant winds are also examined. Similar model domain setups as described in section 3 are used, except that the width of land surface extends from 15 km to 50 km in order to accommodate the long inundation distance induced by the large constant winds. A total of five scenarios are conducted, each with a different combination of constant wind speed and bottom slope of continental shelf (see details in Table A1). The simulation results are summarised in Tables A2 and A3, respectively.

Generally, Tables A2 and A3 show consistent findings with those obtained from TC scenarios, e.g. the combination of wave effects can considerably elevate the maximum storm surge and extend the maximum inundation limit, and among the various wave effects, the wave-breaking induced acceleration (WBA) contributes up to 72% in the total surge height, the wave modified wind stress (WMWS) accounts for 4%-10% of the total surge height, the wave-enhanced bottom friction (WEB) can elevate the storm surge height about 3%, while the momentum flux balance across the air-sea interface (MFB) can reduce the storm surge height by about 1%–9%. In terms of the coastal inundation, it is interesting to note some variations in the relative importance of different wave effects comparing with the TC conditions. With relative small wind speed (i.e. the Exp_N3 with a U_10 of 20 m/s), WBA contributes about 35.5% of the total inundation distance, which shows more important role than WMWS. However, as the wind speed increases, the contribution of WBA to inundation distance decreases while the contribution of WMWS increases, showing the more important role of WMWS in large wind speed conditions. These results from constant wind experiments show overall similar findings as in the TC condition, emphasizing the important role of WMWS and MFB in storm surge level and coastal inundation predictions which require further research.

Table A1. Summary of the numerical test setup.

Scenario	Exp_N1*i**	Exp_N2*i*	Exp_N3*i*	Exp_N4*i*	Exp_N5*i*
BL	1:100	1:100	1:100	1:500	1:1000
U_{10}	60 m/s	40 m/s	20 m/s	60 m/s	60 m/s

Note: * *i* takes the value of [1–5], represents one of the five simulations in a specific scenario as described in Table 1; BL is short for bottom slope and U_{10} represents the 10 meter wind speed.

Table A2. Model calculated maximum storm surge and maximum inundation distance from the constant uniform winds experiment scenarios with different wind speeds (Exp_N1, Exp_N2, Exp_N3).

	Exps (Scenario)	Exp_x1	Exp_x2	Exp_x3	Exp_x4	Exp_x5
MSS (m)	Exp_N1	0.72	1.58	1.62	1.68	1.66
	{U_{10} = 60 m/s}	\	119.44%	2.53%	3.70%	−1.19%
		43.37%	51.81%	2.41%	3.61%	−1.20%
&	Exp_N2	0.49	1.43	1.47	1.57	1.49
Relative Change	{U_{10} = 40 m/s}	\	191.84%	2.80%	6.80%	−5.10%
		32.89%	63.09%	2.68%	6.71%	−5.37%
	Exp_N3	0.13	0.51	0.53	0.55	0.53
	{U_{10} = 20 m/s}	\	292.31%	3.92%	3.77%	−3.64%
		24.53%	71.70%	3.77%	3.77%	−3.77%
MID (m)	Exp_N1	31200	32100	32100	33700	32600
		\	2.88%	0%	4.98%	−3.26%
		95.71%	2.76%	0%	4.91%	−3.37%
&	Exp_N2	20300	21400	21400	22500	21900
Relative Change		\	5.41%	0%	5.14%	−2.67%
		92.69%	5.02%	0%	5.02%	−2.74%
	Exp_N3	2000	3100	2900	3300	3100
		\	55.00%	−6.45%	13.79%	−6.06%
		64.52%	35.48%	−6.45%	12.90%	−6.45%

Table A3. Same with Table A2 but for experiment scenarios with different bed slopes (Exp_N1, Exp_N4, Exp_N5).

	Exps (Scenario)	Exp_x1	Exp_x2	Exp_x3	Exp_x4	Exp_x5
MSS (m)	Exp_N1	0.72	1.58	1.62	1.68	1.66
	{BL = 1:100}	\	119.44%	2.53%	3.70%	−1.19%
		43.37%	51.81%	2.41%	3.61%	−1.20%
&	Exp_N4	1.86	2.64	2.72	3.0	2.75
Relative Change	{BL = 1:500}	\	41.94%	3.03%	10.29%	−8.33%
		67.64%	28.36%	2.91%	10.18%	−9.09%
	Exp_N5	3.93	4.88	5.02	5.43	5.03
	{BL = 1:1000}	\	24.17%	2.87%	8.17%	−7.73%
		78.44%	18.96%	2.79%	8.18%	−8.38%
MID (m)	Exp_N1	31200	32100	32100	33700	32600
		\	2.88%	0%	4.98%	−3.26%
		95.71%	2.76%	0%	4.91%	−3.37%
&	Exp_N4	31700	32500	32400	33500	33000
Relative Change		\	2.52%	−0.31%	3.40%	−1.49%
		96.06%	2.42%	−0.30%	3.33%	−1.51%
	Exp_N5	31900	32700	32500	33500	33000
		\	2.51%	−0.61%	3.08%	−1.49%
		96.67%	2.42%	−0.61%	3.03%	−1.51%